predominated by mechanical vibration and a change in liquid helium pressure, and that the phase fluctuation spectra lie mainly below 1 kHz.

Superconducting crab cavities have been developed at KEK and are being utilized for the crab crossing of the B-factory (KEK-B). Our crab cavity needs little modification, because our RF accelerating frequency is almost the same as that of KEK-B; moreover, our beam current is much smaller than theirs. Taking advantage of our low beam current, we are developing a SPring-8-type tuner with a simple mechanism to improve the reliability and stability of the resonant frequency of the crab cavities.

Developments and Upgrades of Linac

High-Resolution Integrator Circuit for Beam Charge Monitoring [8]

For top-up injection to the SPring-8 storage ring, about every 20 seconds, the linac shoots an electron beam whose beam charge is about 1 nC. In the future, the beam charge will be decreased owing to more frequent beam injection to the storage ring to minimize the stored beam current variation. Presently Fast Gated Integrator and Boxcar Averager Modules (Stanford Research Systems) are equipped as integrator circuits for signal processing. When the beam charge is decreased for the frequent beam injection, the measurement error of the present integrator circuit will be nonnegligible owing to the noise of the integrator. To maintain or improve the resolution, we developed a new integrator circuit to reduce the noise level to 1/10 of the present integrator circuit.

The principle of the new integrator circuit, which is identical as the principle of the present integrator, is as follows: The principal elements are a gate switch and an accumulator (a 6- or 12-m long coaxial cable) connected to a high-impedance sum amplifier as shown in Fig. 23. An input pulse signal is fed to the accumulator via the opened gate switch. When the gate is closed, the input signal is confined in the accumulator, that is, the signal repeats reflections at both ends of the accumulator. As a result, the signal pulse becomes dull in shape and is averaged as the signal transfers forward and backward. This averaged voltage is proportional to the integral of the signal voltage while the gate is open.

The S/N ratio at the accumulator stage can be maximized by minimizing the length of the accumulator that affects the signal attenuation. The minimum accumulator length is determined on the basis of the pulse width of the input signal including the rise and fall times of the gate switch. We have therefore focused on enhancing the transient response of the gate switch.

A transfer switch (SW-283-PIN, M/A-COM) was adopted as the gate switch to terminate all ports for eliminating switching noises generated at an open port. The rise time of the gate switch is determined from the root sum square of the rise times of the transfer switch and the control voltage. To avoid lengthening the rise time of the gate switch, a fast circuit was developed to generate control voltages for

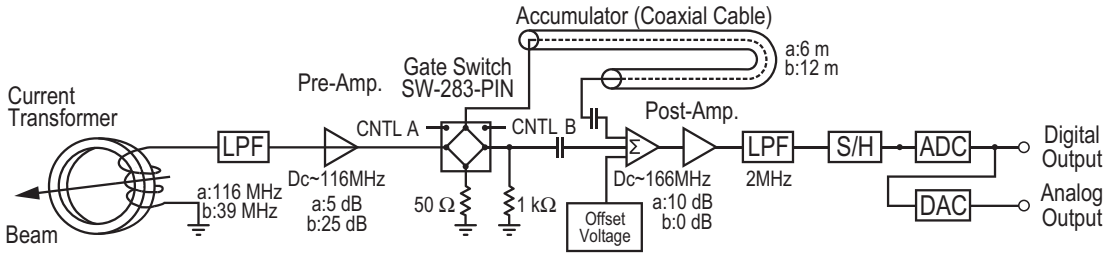

Fig. 23. Block diagram of developed integrator circuit. "a:" denotes the parameter for a short (1 ns) pulsed beam measurement, while "b:" denotes the parameter for a long (40 ~ ns) pulsed beam measurement.

the transfer switch. The circuit is composed of a transistor bridge circuit and clipping diodes as shown in Fig. 24. The control voltages of -0.1 and -7.9 V are instantaneously inverted by the external gate pulse. We finally obtained the rise time of 2 ns (10-90%).

The resolution of the developed integrator circuit was measured as 0.65 pC under conditions of a range of 2 nC and a gate width of 20 ns, that is, the resolution of the developed integrator circuit has been significantly improved to 1/12 of that of the present integrator with the same range and gate width conditions. The linearity of the output voltage to the time integral of the input voltage was measured with a gate width condition of 20 ns. The obtained output voltages showed good linearity with its deviation of 0.14% rms. The observed performance of the integrator sufficiently satisfies our requirement for the future low-current operation of the linac.

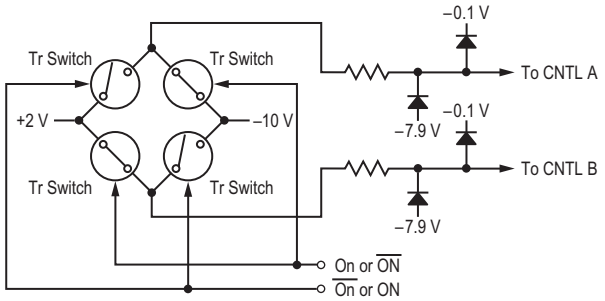

Fig. 24. Block diagram of the circuit to generate control voltages for SW-283-PIN.

RF Gun Development

Upgrade of 3D UV laser pulse shaping system

To minimize the beam emittance of a photocathode RF gun, the laser pulse shape should be optimized in three dimensions. One of the candidates for a reliable 3D laser pulse shape was the cylindrical beer-can-shaped (spatially top-hat and temporally square) pulse. The 3D UV laser pulse shaping system combined with a deformable mirror (transverse: 2D) assisted by a genetic algorithm and a chirped pulse stacker (longitudinal: 1D) was completed at SPring-8.

In 2007, we installed a new UV pulse stacking system that consisted of three birefringent α-BBO crystal rods [9] to fix the optical delays between neighboring microchirped pulses in the previously developed mechanical pulse stacker [10]. To avoid the interference caused by stacking, orthogonally polarized chirped pulses are alternatively stacked with an optical delay. The optical delay period should be 1.2~1.3 times longer than the microchirped pulse duration to generate a homogeneous electron bunch at the cathode. This method, which introduces additional chirp to avoid interference, as shown in Fig. 25, is referred to as “chirped pulse stacking” [10]. The optimal chirp of a micropulse minimizes interference caused by stacking to make the plateau of a combined pulse flat. This chirping was carried out with group delay dispersion (GDD) in whole transport optics and additional adjustable chirping introduced by DAZZLER (AO-modulator) at the fundamental wavelength.

A birefringent crystal that resembles a conventional retardation plate works on the basis of a principle for time delay. It does introduce a certain temporal delay between two orthogonally polarized components of a linearly polarized incident beam. The angle of rotation of each crystal axis against incident polarization is 45° to make twin pulses. Then a pulse train with equivalent intervals is connected smoothly with additional pulse stretching introduced by DAZZLER (Fig. 25). These α-BBO crystal rods can be used as a pulse stacker in the super broadband wavelength region (189−3500 nm). To obtain the longest square laser pulse duration of 32 ps with four birefringent crystals, the crystals must generate temporal delays of Δt=2.0, 4.0, 8.0, and 16 ps. The 4-, 8-, or 16-ps squarely combined pulse is generated by rotating the crystal axis parallel to the incident polarization at each corresponding crystal as shown in Fig. 25.

Proposal of Z-polarization Schottky emission gun with hollow laser incidence

By focusing a radial polarized beam on the photocathode (Fig. 26), the laser’s electric field is generated in the laser propagation direction (Z-direction) at the focus point. The Z-field oscillates with a periodic time of ~2.6 fs at the fundamental Ti:Sapphire laser light (~790 nm), for example. By introducing a hollow laser incidence, the generated Z-polarization field can exceed an electrical field of 1 GV/m even with a fundamental wavelength from compact femtosecond Ti:Sapphire laser systems. In a 1 GV/m field, the work function of the copper cathode decreases by ~2 eV [11]. This Schottky effect can be used as a gate of the photoemission process. Thus, a laser-induced Schottky-effect-gated photocathode gun using the Z-polarization of the laser source was proposed [11] as a future multi-bunch high brightness electron source with a low charge.

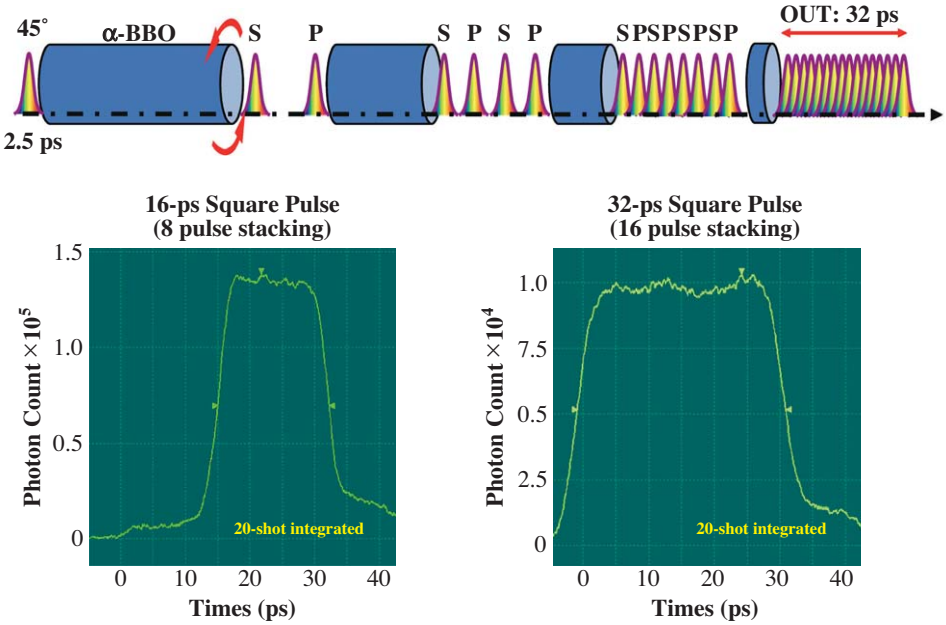

Fig. 25. Measurement results obtained using a streak camera (Fesca-200) of UV-laser pulses stacked with BBO crystal rods. For instance, the rotation angle of the first crystal rod against incident polarization works as a half waveplate in our mechanical pulse stacker. By rotating the first crystal rod, switching between 16- and 32-ps square pulses is available.

We have conducted a feasibility study of this laser-induced Schottky effect on the photocathode by comparing radial and azimuthal polarizations. In this experiment, the linear polarization of the incident laser only switches from the vertical to the horizontal direction. Note that we can keep the same photon densities at the focus point during experiments comparing radial and azimuthal polarizations. In this method, we can separately verify the Schottky effect due to the Z-field from the multiphoton process.

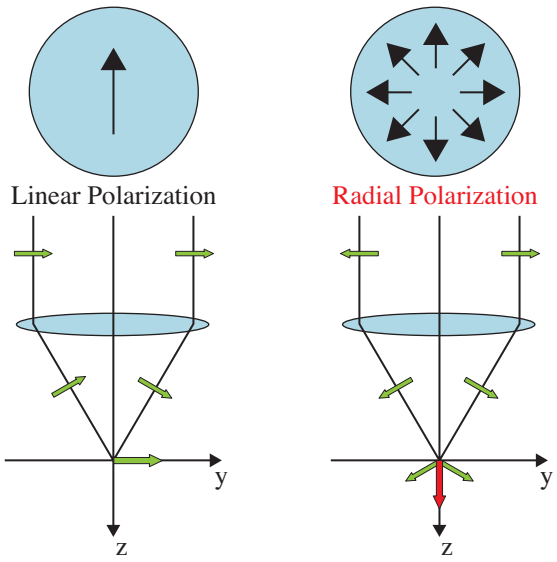

Fig. 26. Principle of Z-polarization optical field on cathode generated from radial polarization.

Haruo Ohkuma*, Hiroto Yonehara, Hirofumi Hanaki

SPring-8/JASRI

*E-mail: ohkuma@spring8.or.jp

References

[1] SPring-8 Research Frontiers 2006, p. 179.
[2] SPring-8 Research Frontiers 2007, p. 188.
[3] K. Soutome *et al.*: Proc. EPAC08 (2008), p. 3149.
[4] M. Oishi *et al.*: SPring-8 Internal Report, SR06-007 (in Japanese).
[5] T. Bizen: Nucl. Instrum. Meth. A **574** (2006) 401.
[6] SPring-8 Research Frontiers 2006, p183.
[7] SPring-8 Research Frontiers 2007, p195.
[8] K. Yanagida *et al.*: Proc. LINAC08 (2008) - to be published.
[9] H. Tomizawa *et al.*: Proc. FEL07 (2007), p. 298.
[10] H. Tomizawa *et al.*: Quantum Electronics **37** (2007) 697.
[11] H. Tomizawa and M. Kobayashi: Proc. FEL07, p. 382.